JOURNAL OF GEOPHYSICAL RESEARCH, VOL. 105, NO. B10, PAGES 23,403–23,420, OCTOBER 10, 2000

Three-dimensional structure of the Torngat Orogen (NE Canada) from active seismic tomography

Thomas Funck,[1] Keith E. Louden,[1] Richard J. Wardle,[2] Jeremy Hall,[3] James W. Hobro,[4] Matthew H. Salisbury,[5] and Angelina M. Muzzatti[6]

Abstract. The crustal velocity structure and the Moho depth of the Proterozoic Torngat Orogen, NE Canada, is determined by active seismic tomography using travel times of crustal turning rays and Moho reflections. The orogen developed during oblique convergence of the Archean Superior and Nain Provinces, which trapped an interior belt of Archean crust (Core Zone) between them, with the Torngat Orogen evolving between the Core Zone and the Nain Province. Beneath the central orogen a crustal root is found with a preserved depth of >52 km and a width of ~100 km. To the north, the root shallows to <44 km and narrows to a width of ~45 km. The root correlates with a set of major, late orogenic shear zones that accommodated oblique convergence of the Superior and Nain Provinces. This correlation suggests that the transpressional shearing focused strain in the region of the root and contributed to the crustal thickening. Absence of postorogenic magmatic activity prevented reworking or thermal relaxation of the root. The lack of late magmatism is probably related to the depleted and refractory nature of the Archean lithosphere underlying the orogen. Upper crustal velocities are lowest in the Core Zone (~5.7 km/s at the surface) and are compatible with laboratory measurements carried out on gneissic rock samples from that area. Higher velocities in the Nain Province (~5.9 km/s) correlate with felsic gneiss and anorthosite rock samples. A high-velocity region immediately to the north of the crustal root is associated with a Moho uplift (~34 km). This is explained by extension along the Ungava transform fault, and possibly in Hudson Strait, at ~55 Ma when rifting in the Labrador Sea was transferred into Baffin Bay.

1. Introduction

Seismic studies have revealed a number of preserved crustal roots in the closely related Paleoproterozoic orogenic belts of Laurentia [*Lucas et al.*, 1993; *Funck and Louden*, 1999] and Baltica [*Grad and Luosto*, 1987; *BABEL Working Group*, 1990]. While the preservation of these roots for >1.5 Gyr is commonly related to the absence of postorogenic heating, there is a range of explanations for their creation. Some are thought to represent frozen subducted slabs [*BABEL Working Group*, 1990], and others are interpreted to result from ductile reworking of thickened crust during postcollisional transpression [*Németh et al.*, 1996] or from delamination of lithosphere and subsequent thickening of the crust by underplating [*Nironen*, 1997].

The Torngat Orogen has been studied as part of Lithoprobe's Eastern Canadian Shield Onshore-Offshore Transect (ECSOOT). A previous refraction/wide-angle reflection (R/WAR) seismic transect across the Torngat Orogen (ECSOOT96 line 5W-E, Figure 1) found evidence for the existence of a crustal root beneath the orogen [*Funck and Louden*, 1999]. However, the experiment could not provide a definitive answer as to how the root was formed because of the lack of information about the three-dimensional (3-D) geometry of the root. It is clear that the root does not have a simple 2-D shape since an earlier reflection seismic line (ECSOOT92, Figure 1) shows no evidence for a root 200 km to the north of the R/WAR seismic transect [*Hall et al.*, 1995]. The seismic tomography study presented in this paper was designed to obtain more detailed information about the crustal thickness and structure for large parts of the orogen and to allow for a correlation with the complex geology in the area. The results from the tomography are compared with velocities obtained from rock samples from the study area and with potential field data. Together with geological data, an integrated interpretation for the orogenic development of the Torngat Mountains will be given.

2. Geological Setting

The southeastern Churchill Province in northeastern Canada (Figure 1) has a basic tripartite subdivision consisting of an interior belt of Archean crust, known as the Core Zone, and the bordering Archean cratons of the Nain and Superior Provinces [*Wardle*, 1998]. The Core Zone is linked to the

[1]Department of Oceanography, Dalhousie University, Halifax, Nova Scotia, Canada.
[2]Geological Survey, Newfoundland Department of Mines and Energy, St. John's, Newfoundland, Canada.
[3]Department of Earth Sciences, Centre for Earth Resources Research, Memorial University of Newfoundland, St. John's, Newfoundland, Canada.
[4]Bullard Laboratories, Department of Earth Sciences, University of Cambridge, Cambridge, England, United Kingdom.
[5]Geological Survey of Canada, Bedford Institute of Oceanography, Dartmouth, Nova Scotia, Canada.
[6]Department of Earth Sciences, Dalhousie University, Halifax, Nova Scotia, Canada.

Paper number 2000JB900228.
0148-0227/00/2000JB900228$09.00

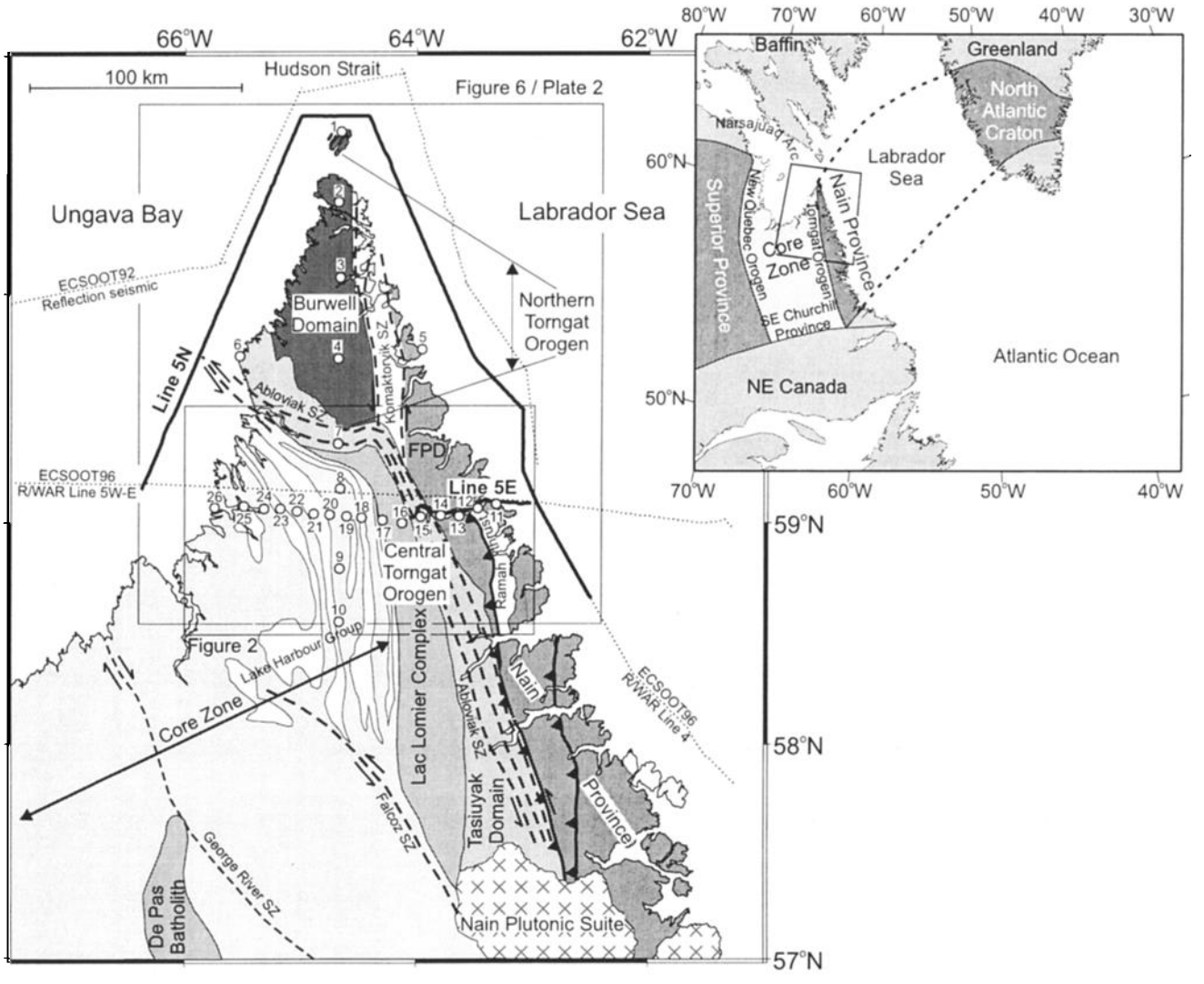

Figure 1. Simplified geological map of the study area [after *Hall et al.*, 1995], showing the location of the seismic tomography experiment (lines 5N and 5E). Solid lines show the air gun shots, and circles indicate the location of the seismic land stations. Dotted lines show the location of other seismic profiles relevant to this study, as mentioned in the text. Solid lines with triangles mark thrust faults, dashed lines show shear zones (SZ), and arrows indicate the sense of displacement. FPD is Four Peaks domain. The inset shows the geological provinces in northeastern Canada and the correlation of the Nain Province with the Archean block of Greenland.

cratons by the Paleoproterozoic supracrustal belts of the New Quebec and Torngat Orogens. Tectonic units in the study area of the Torngat Orogen are briefly described below from west to east.

The Core Zone is predominantly Archean in age (3.0-2.6 Ga) [*Ryan et al.*, 1991; *Machado et al.*, 1989; *Isnard et al.*, 1998] with some infolded Paleoproterozoic metasedimentary rocks of the Lake Harbour group in the northeast [*Dunphy and Skulski*, 1995]. The enigmatic 1.84-1.82 Ga granitoid plutons of the Lac Lomier complex [*Scott*, 1997] are thought to form a southeast extension of the Narsajuaq arc [*Scott and St-Onge*, 1998]. The Tasiuyak domain is a metasedimentary gneiss with a depositional age of 1.94-1.895 Ga [*Scott and Gauthier*, 1996] that probably represents an accretionary prism [*Wardle and Van Kranendonk*, 1996]. The Burwell domain is interpreted as a subduction related magmatic arc ranging in age from 1.91 to 1.86 Ga [*Scott*, 1995a]. It comprises a series of quartz diorite to granite plutons of overall calc-alkalic character [*Van Kranendonk and Wardle*, 1997] intruded at least partly into a substrate of Archean crust. The Nain Province is composed of Archean gneisses with the Four Peaks domain lying in the Torngat foreland [*Wardle and Van Kranendonk*, 1996].

The formation of the Torngat Orogen is characterized by three main deformational events (D1-D3). The first phase D1 from 1.86 to 1.85 Ga [*Bertrand et al.*, 1993] was associated with the initial collision and resulted in the burial of the Core Zone beneath the overthrusting Nain crust. D2 deformation (1.84-1.82 Ga) was transpressional and associated with formation of the sinistral Abloviak and Falcoz shear zones [*Scott*, 1998; *Bertrand et al.*, 1993; *Van Kranendonk*, 1996]. The last phase of deformation (D3) from 1.8 to 1.74 Ga [*Scott and Machado*, 1995] was partitioned into northern and central components. In the north, D3 resulted in the southward indentation of the Burwell domain into the Core Zone, which was accommodated by sinistral motion on the Komaktorvik

shear zone [*Bertrand et al.*, 1993] and by bending of the Abloviak shear zone. The resulting westward offset of the Abloviak shear zone divides the Torngat Orogen into a northern and central part. In the central Torngats, D3 was associated with strong east directed thrusting (Ramah thrust) and westerly directed nappe-style folding [*Wardle and Van Kranendonk*, 1996; *Goulet and Ciesielski*, 1990].

Subsequent to the orogeny, the southern Torngat Orogen was affected by a period of Mesoproterozoic anorogenic plutonism forming the 1.3 Ga Nain Plutonic Suite [*Emslie et al.*, 1994]. The Nain Province forms the western part of the North Atlantic craton (NAC) that can be correlated with the Archean block in southern Greenland [*Sutton et al.*, 1972; *Bridgwater et al.*, 1973; *Bridgwater and Schiøtte*, 1991]. The NAC was a continuous structure prior to the Mesozoic rifting [*Srivastava*, 1978; *Roest and Srivastava*, 1989] that created the Labrador Sea between Greenland and North America.

3. Experiment and Data

The ECSOOT96 active seismic tomography experiment covers the northern and central Torngat Orogen between Ungava Bay and Labrador Sea (Figure 1). The seismic source was an array of six air guns (volume of 16.4 L each) towed by CSS *Hudson*. The frequency spectrum of the recordings shows that the main seismic energy lies between 2 and 10 Hz with peak power around 5 Hz. Shots on line 5N were fired along three segments parallel to the coast of the Torngat peninsula in northern Labrador. The segment in Ungava Bay comprises 1189 shots, the E-W segment in Hudson Strait consists of 308 shots, and in the Labrador Sea, 1735 shots were fired. In addition, 405 shots from line 5E in the Nachvak Fiord were included in the data set, providing some quasi-onshore shots. The length of the shot lines is 552 km resulting in an average shot spacing of 152 m. A total of 26 three-component 4.5-Hz geophone seismic recorders were deployed by helicopter to record the shots, with the station elevation varying between 5 and 798 m. Stations 1 to 6 were Dalhousie-designed seismometers with a sampling rate of 87.1 Hz, and stations 7 to 26 were instruments manufactured by REFTEK with a sampling rate of 100 Hz. Station 5 was disturbed by a polar bear, and data from station 9 could not be retrieved. Air gun shots were located using smoothed GPS navigation (error <50 m) and positions of land stations were determined by differential correction to raw GPS locations (error <2 m). The absolute timing of land stations and air gun shots was done by synchronization with the GPS time signal assuming a linear drift between clock checks.

During the seismic experiment, 23 rock samples were collected along the central Torngat Orogen (Figure 2) for laboratory analysis of their seismic velocities. The samples were taken from outcrop or autochthonous float representing the major lithologies in that area. The lithology of the samples ranges from felsic rocks such as granites, tonalite gneisses, paragneiss, and psammitic gneiss to mafic rocks such as mafic gneiss, anorthosites, and basalt dikes.

4. Methodology

4.1. Seismic Tomography

The digital seismic recordings were converted to SEG-Y format using IRIS-PASSCAL (Incorporated Research Institutions for Seismology - Program for Array Seismic Studies of the Continental Lithosphere) and in-house software. One example for a record section is shown in Figure 3. First arrivals are usually crustal turning rays (P_g) except for large shot-receiver distances (>170 km), where refracted waves through the upper mantle (P_n) arrive first. The Moho reflection (P_mP) appears as a high-amplitude second arrival, whereas crustal reflections (P_iP) have lower amplitudes. For the seismic tomography, travel times of P_g and P_mP phases were used. The P_n phase was not included in the inversion because it was only recorded by the southern stations for shots in Hudson Strait. This shot-receiver distribution has only a few crossing ray paths in the mantle. The P_iP phase was not included because it could only be safely identified on a few records. This is due to the low amplitude of the phase and the off-line (fan) geometry of the shots. Hence the crust was treated as a single layer with a smoothly varying velocity structure.

The picking of arrival times was done with the interactive program ZPLOT (C. A. Zelt, personal communication, 1998). Pick uncertainties ranging from 50 to 150 ms were assigned to each travel time pick. The close shot spacing of 152 m results in some redundancy of the data. For this reason, only every fifth shot was included in the inversion. In total, 9939 P_g and 5539 P_mP travel time picks were used.

For the computation of a three-dimensional minimum-structure model, the program JIVE3D was used [*Hobro*, 1999], which is based on the 2-D-inversion algorithm of *McCaughey and Singh* [1997]. This program allows simultaneous velocity and interface tomography using travel times of reflected and refracted seismic phases. The forward problem is solved using a ray tracing method based on that of *Farra* [1990]. This method uses ray perturbation theory to allow rapid ray tracing through smooth velocity functions. Ray fans are sent out from the receivers at various azimuths and takeoff angles. The travel time to a particular shot point is calculated by interpolation of the travel time trajectories and tracing of the final rays to check that the interpolation was sound. For the inversion a least squares minimization of the travel time residuals is used. To ensure that the solution of the inversion is well posed and plausible, the model is regularized by its smoothness. The inversion starts with a highly

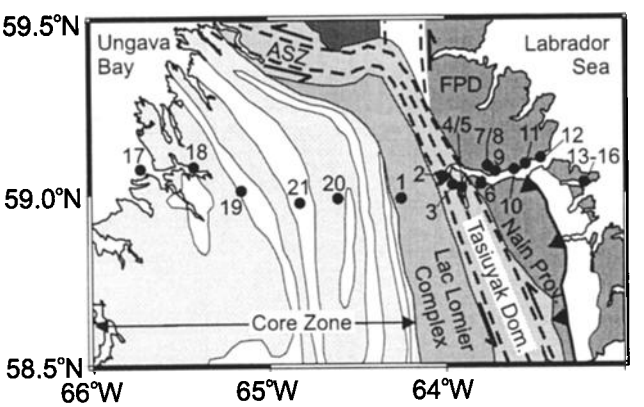

Figure 2. Geological map of the central Torngat Orogen, showing the location of the rock samples (circles). FPD is Four Peaks domain, ASZ is Abloviak shear zone, Dom. is Domain and Prov. is Province.

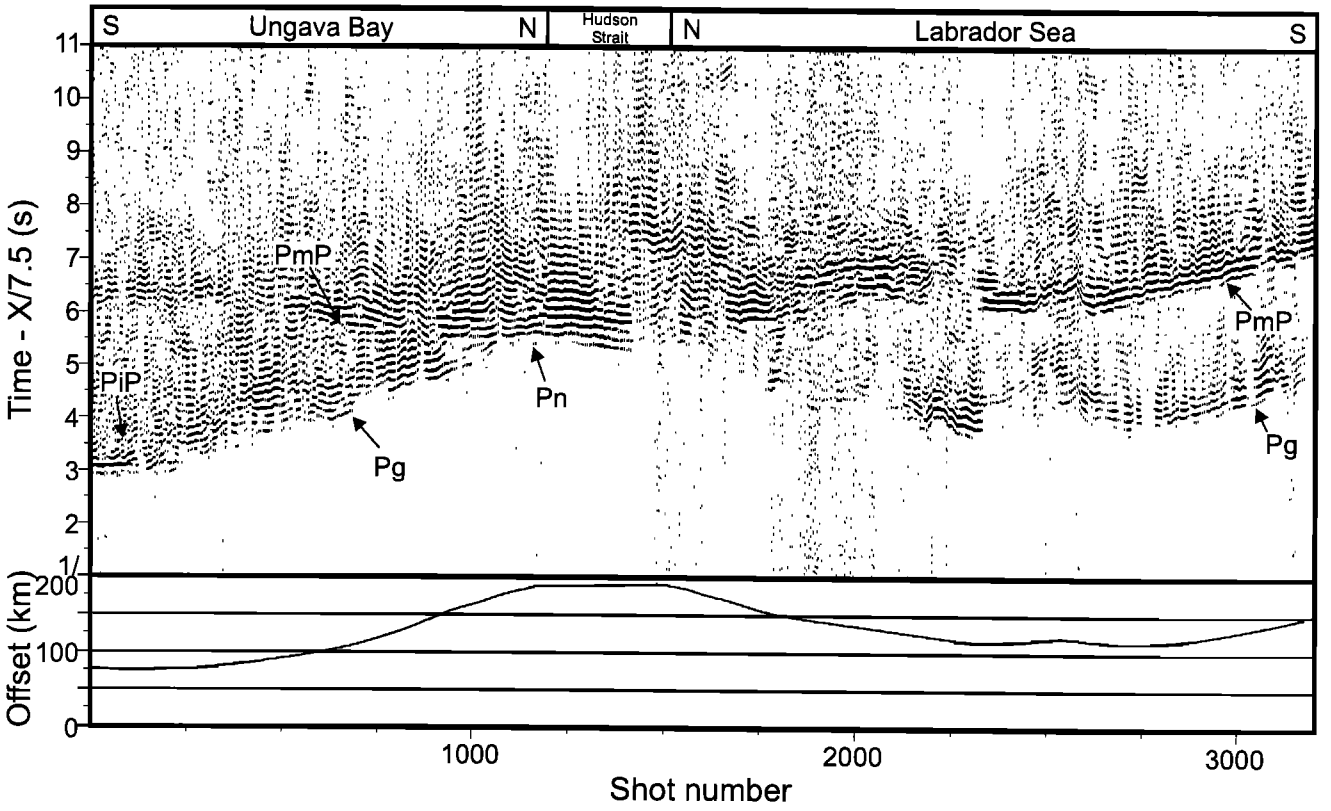

Figure 3. Record section (top) for station 22 recording the shots on line 5N. Horizontal scale is shot number, with shots 1 through 1189 in Ungava Bay, shots 1190 through 1497 in Hudson Strait, and shots 1498 through 3232 in Labrador Sea. The vertical scale for the record section is the travel time using a reduction velocity of 7.5 km/s. The section is displayed with a band-pass filter (4-10 Hz) and trace normalization. The graph in the bottom shows the shot-receiver distance (offset) for each shot.

smoothed model and then allows this to fit the large-scale general trends in the data by applying tight regularization. Later, the regularization strength is gradually relaxed until sufficient structure has emerged to explain the data within the uncertainties.

For the parameterization of the inversion the subsurface was mapped as a single crustal velocity layer bounded by interfaces representing the surface and the Moho (Figure 4). Because of the shallow water in the study area (depths between 16 and 421 m with an average of 201 m), shots were projected to the seafloor rather than introducing a separate water layer. Travel times were corrected by applying a water velocity of 1500 m/s. The upper boundary in the model is the combined land surface and seafloor. This interface is defined along a regular grid with a horizontal node spacing of 1 km and was computed from the elevation of the seismic receivers, water depth along the shot lines, ETOPO5 water depths [*National Geophysical Data Center, 1988*] and GTOPO30 land elevations [*U.S. Geological Survey, 1996*]. The lower boundary represents the Moho, which was defined along a grid with a horizontal spacing of 5 km. Moho depth in the starting model was 38 km. The nodes defining the Moho were allowed to move vertically during the inversion, whereas the nodes of the surface layer were fixed. Velocities within the crustal layer were defined on a grid with a node spacing of 10

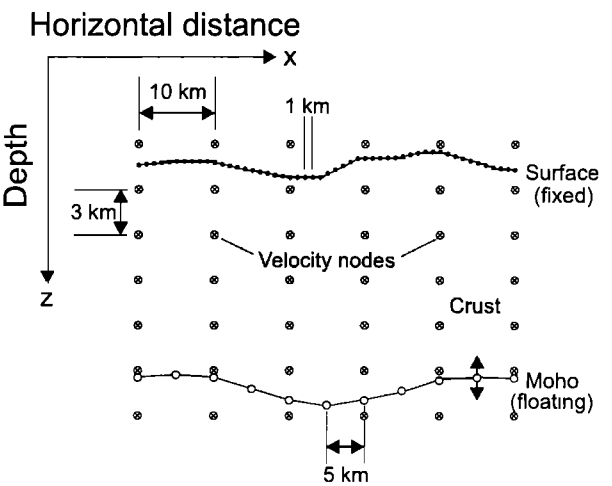

Figure 4. Vertical cross section showing the setup of grid nodes used for the inversion. Crustal velocities are defined along a regular grid (circles with crosses) with a horizontal spacing of 10 km and a vertical spacing of 3 km. The upper boundary of the crust is given by the surface geometry (seafloor/topography) using a horizontal grid node (solid dots) spacing of 1 km. The lower boundary of the crust is determined by the Moho geometry with a horizontal grid node (open circles) spacing of 5 km.

km in the horizontal direction and 3 km in the vertical direction. A constant velocity gradient was used for the starting model with a velocity of 5.8 km/s at sea level and 6.86 km/s at 38 km. These velocities and the Moho depth are of the order of values found for relatively pristine Archean crust in the area [*Funck and Louden*, 1998; 1999].

Variations in Moho depth between 35 and 50 km [*Funck and Louden*, 1999] were known in the study area, and P_mP travel time residuals in the starting model with a constant Moho depth of 38 km were often substantial. To stabilize the inversion, the first 12 iterations only inverted for the Moho depth to obtain the long-wavelength (wavelengths >80 km) geometry of the crust-mantle boundary. The following 50 iterations jointly inverted for Moho depth and crustal velocities using the updated model from the previous iteration step as input model for the next iteration. During this process the regularization strength was reduced after each 10 iterations. The first set of iterations allowed velocity structure to develop with horizontal wavelengths of >280 km and >80 km for the Moho geometry. For the last iteration, velocity structure with wavelengths >25 km and Moho structure with wavelengths >15 km could develop. The final misfit normalized by the pick uncertainty (χ^2) was 1.2, and the travel time residual t_{rms} was 93 ms. This model was chosen as the final model because it represents the model with the minimum structure necessary to explain the observed travel time data. Continuing the inversion with a less tight regularization resulted in small-scale features without reducing the data misfit. For the gridding and display of the results Generic Mapping Tools (GMT) software was used [*Smith and Wessel*, 1990; *Wessel and Smith*, 1991].

4.2. Rock Sample Velocity Measurements

Seismic velocity measurements on the rock samples were performed at the Dalhousie University/Geological Survey of Canada high-pressure testing facility located at Dalhousie University. Surficially weathered samples were trimmed and minicores ranging from 2.8 to 5 cm in length with a diameter of 2.5 cm were drilled. Depending on whether or not the sample contained foliation and lineation, up to three oriented minicores were taken to test for anisotropy. If the sample displayed foliation, one core was extracted parallel to the foliation and one perpendicular to the foliation. From samples with both foliation and lineation, three cores were taken, one perpendicular to the foliation, one parallel to both the foliation and lineation, and one parallel to the foliation but perpendicular to the lineation.

After the sample preparation, the dimensions and masses of the cores were measured using a digital vernier caliper and a top loading balance (precision ±0.01 g). Compressional and shear wave velocity measurements were performed under dry conditions at hydrostatic confining pressures ranging from 20 to 600 MPa using the pulse transmission technique of *Birch* [1960]. Velocities were compiled from the lengths of the minicores and the travel times of P and S waves through the samples.

5. Results

5.1. Rock Sample Velocities

The results of the laboratory P wave and S wave velocity measurements on the rock samples are summarized in Tables 1 and 2, respectively. All samples show an initial sharp increase in P wave velocity with increasing pressure due to the rapid closure of microcracks and pore spaces (Figure 5). Above 200 MPa the velocity-pressure relationship for most of the samples becomes essentially linear. This is thought to be due to the closure of microcracks and pore spaces in the rock [*Birch*, 1961]. Velocities determined at higher pressures are representative of the mineralogy and the orientation of mineral grains. Velocities at 20 MPa range from 4.80 km/s (sample L19, granitoid gneiss) to 6.94 km/s (L8b, mafic gneiss). At 600 MPa the slowest sample is a quartzite with a compressional wave velocity (v_p) of 6.08 km/s (sample L16), while the fastest is mafic gneiss with v_p equal to 7.24 km/s (sample L8b). Mafic rock samples are characterized by velocities >6.8 km/s at 600 MPa and densities >2950 kg/m^3, while the felsic and intermediate samples tend to have lower velocities and densities.

The Poisson's ratios were calculated from the P and S wave velocities at 600 MPa and generally range from 0.204 to 0.284 (Table 1). Two samples with a high quartz content have lower Poisson's ratios. The quartzite (sample L16), which has a quartz content of 95%, has a value of 0.106 and a biotite-quartz-feldspar (bio-qtz-fs) gneiss (sample L21) with 50% quartz has a Poisson's ratio of 0.177. Six rock samples have a P wave anisotropy of >4%. Four of those six samples are rather felsic (L2, L7, L12, and L 17), while two are mafic (L8b and L14). For comparison with the velocities obtained from seismic tomography the rock sample velocities were converted from pressure to depth by using an average density of 2800 kg/m^3.

5.2. Velocity Cross Sections

Crustal P wave velocities from the seismic studies within the northern and central Torngat Orogen are displayed in horizontal (Figure 6), and vertical (Plate 1) cross sections. On the horizontal sections a clear correlation with the surface geology is discernible. At sea level (z=0 km, Figure 6) velocities are lowest in the Core Zone and the Burwell domain with values between 5.6 and 5.8 km/s. Higher velocities (5.8 to 6.0 km/s) are found in the Komaktorvik shear zone and the Nain Province.

Two higher-velocity areas can be identified. One is located in the Four Peaks domain of the Nain Province with velocities of ~6.1 km/s and correlates with high-velocity rock samples (L7, L8b, and L9) in that area (Table 1). The other high-velocity region (~6.1 km/s) is located in the northern part of the Burwell domain and does not correlate with geological structures at the surface. In the area of the easternmost land station (station 11) a small lower-velocity area (<5.8 km/s) can be found within the Nain Province. Four rock samples (L13-L16) were collected in this zone with two of them showing rather low velocities (a felsic gneiss and a quartzite). The other two (a mafic gneiss and a basalt) are characterized by high velocities but are not common in the area. A coinciding R/WAR seismic line in the low-velocity region [*Funck and Louden*, 1998] indicates a Poisson's ratio of 0.20 for the area, which was interpreted to be related to a high quartz content. This Poisson's ratio falls between those of the two low-velocity rock samples (0.106 for the quartzite and 0.247 for the felsic gneiss) and would suggest that the major lithology is a felsic gneiss with a high quartz content.

At a depth of 5 km (Figure 6) another low-velocity region with velocities as low as 5.5 km/s can be seen in the Labrador

Table 1. Physical Properties of Rock Samples From the Central Torngat Orogen

Sample	Lithology	P Wave Velocity at Pressure, km/s										Poisson's Ratio	Anisotropy, %	Density, kg/m^3
		20 MPa	40 MPa	60 MPa	80 MPa	100 MPa	200 MPa	300 MPa	400 MPa	500 MPa	600 MPa			
L1	tonalite gneiss	5 995	6.070	6.135	6.200	6.428	6.383	6.454	6.489	6.510	6.520	0.284	0.15	2680
L2	paragneiss	5.647	6.137	5.983	6.077	6.142	6.322	6.380	6.423	6.465	6.502	0.207	6.17	2810
L3	felsic gneiss	5.273	5.600	5.797	5.942	6.042	6.337	6.473	6.543	6.595	6.650	-	3.01	2827
L4	felsic gneiss	5.986	6.043	6.081	6.109	6.126	6.188	6.233	6.262	6.284	6.313	0.238	1.22	2627
L5	mafic gneiss	6.578	6.719	6.771	6.806	6.833	6.901	6.940	6.975	7.006	7.033	0.276	3.27	2980
L6	anorthosite	5.545	5.823	5.983	6.085	6.142	6.265	6.323	6.364	6.399	6.435	0.259	0.31	2800
L7	felsic gneiss	6.117	6 282	6.377	6.427	6.464	6.567	6.605	6.627	6.643	6.659	-	4.66	2793
L8b	mafic gneiss	6.942	7.002	7 041	7.068	7.088	7.150	7.177	7.200	7.222	7.243	0.252	6.36	3103
L9	dike	6 440	6.527	6 567	6.595	6.617	6.675	6.710	6 740	6.765	6.793	0 266	-	3000
L10a	felsic gneiss	5 308	5.593	5.745	5.838	5.900	6.041	6 102	6.150	6.199	6.242	0.240	2.08	2685
L10b	felsic gneiss	5.618	5.750	5.817	5.868	5.909	6.008	6.044	6.077	6.109	6.142	0.213	1.14	2805
L11a	felsic gneiss	5.510	5 790	5.890	5.963	6.020	6.164	6.235	6.294	6.353	6.413	0.243	0.23	2695
L11b	mafic gneiss	6.320	6.493	6.573	6.628	6.676	6.828	6.903	6.943	6.970	6.993	0.247	3.65	3060
L12	granite	5.745	6.078	6.213	6.277	6.324	6.449	6.507	6.539	6.562	6.580	0.247	4.57	2625
L13	felsic gneiss	5.155	5.510	5.730	5.841	5.913	6.098	6.192	6.238	6.273	6.305	0.247	1 74	2620
L14	basalt dike	6.773	6.845	6.893	6.930	6.960	7.061	7.115	7.139	7.153	7.167	-	4 93	3055
L15	mafic gneiss	6.050	6.370	6.515	6.615	6.693	6 928	7.041	7.087	7.119	7.146	0.264	0 25	3070
L16	quartzite	5.180	5.490	5.630	5.710	5.765	5.905	5.975	6.013	6.045	6.079	0.106	-	2680
L17	granitoid gneiss	4.797	5.193	5.505	5.722	5.855	6.132	6.237	6.297	6.340	6.386	-	7.08	2727
L18	marble	6.200	6.540	6.630	6.690	6.727	6.825	6.885	6.930	6.965	6.997	0.278	-	2860
L19	psammitic gneiss	5.620	5.712	5.805	5.872	5.922	6.070	6.125	6.165	6.198	6.227	0.204	2.14	2715
L20	granitoid gneiss	5.295	5.565	5.773	5.915	6.030	6.270	6.355	6.410	6.463	6.514	0.239	1.87	2890
L21	bio-qtz-fs gneiss[a]	5.363	5.700	5.830	5.900	5.945	6.051	6.087	6.120	6.153	6.186	0.177	1.26	2660

[a] bio, biotite; qtz, quartz; fs, feldspar.

Table 2. Shear Wave Velocities of Rock Samples from the Central Torngat Orogen

Sample	Lithology	S Wave Velocity at Pressure, km/s									
		20 MPa	40 MPa	60 MPa	80 MPa	100 MPa	200 MPa	300 MPa	400 MPa	500 MPa	600 MPa
L1	tonalite gneiss	3.420	3.460	3.485	3.503	3.517	3.558	3.576	3.580	3.582	3.584
L2	paragneiss	3.578	3.676	3.731	3.775	3.795	3.878	3 915	3.929	3.941	3.953
L4	felsic gneiss	3.595	3.622	3.640	3.652	3.662	3.685	3.691	3 694	3.697	3.700
L5	mafic gneiss	3.750	3.788	3.813	3.828	3.842	3.872	3.888	3.899	3.906	3 913
L6	anorthosite	3.400	3.490	3.527	3.553	3.573	3.623	3.638	3 648	3.660	3.670
L8b	mafic gneiss	4.005	4.040	4.057	4.069	4.078	4.102	4.112	4.120	4.127	4.168
L9	dike	3.720	3.755	3.770	3.782	3.790	3.808	3.816	3.822	3.830	3.838
L10a	felsic gneiss	3.345	3.430	3.461	3.486	3.505	3.565	3.594	3.613	3.632	3.653
L10b	felsic gneiss	3.438	3.531	3.571	3.598	3.615	3.650	3.665	3.679	3.692	3.709
L11a	felsic gneiss	3.350	3.490	3.530	3.560	3.580	3.647	3.680	3.699	3.717	3.735
L11b	mafic gneiss	3.812	3.868	3.898	3.919	3.937	3.991	4.016	4.029	4.043	4.055
L12	granite	3.470	3.590	3.643	3.675	3.698	3.759	3.781	3.792	3.803	3.814
L13	felsic gneiss	3.340	3.423	3.464	3.492	3.511	3.567	3.588	3.610	3.632	3.654
L15	mafic gneiss	3.666	3.803	3.884	3 918	3 941	3.994	4.014	4.026	4.036	4.048
L16	quartzite	3.660	3.782	3.855	3.895	3.914	3 977	4.007	4.016	4.025	4.037
L18	marble	3.600	3.685	3.729	3.756	3.775	3.828	3.848	3.858	3.869	3.879
L19	psammitic gneiss	3.455	3.552	3.602	3.631	3.653	3.723	3.757	3.770	3.784	3.798
L20	granitoid gneiss	3.489	3.571	3 633	3.690	3.719	3.782	3.794	3.800	3.806	3.813
L21	bio-qtz-fs gneiss[a]	3.415	3.612	3.697	3.740	3.766	3.831	3.849	3.858	3.867	3.877

[a] bio, biotite; qtz, quartz; fs, feldspar.

Sea, where the shot line extends farther offshore. The westward limit of this low-velocity region correlates with the landward edge of the Mesozoic sediments on the Labrador margin [*Hall et al.*, 1995]. Therefore the low-velocity zone is interpreted to be related to sediment infill in that region. However, the velocities in that zone are higher than those of typical sediments. This is related to the spacing of the velocity nodes in the model (10 km horizontal and 3 km vertical spacing), which is too coarse to determine the exact shape and velocity structure of the possibly thin sediment layer. However, the travel time delays of shots in areas covered with sediments can be explained sufficiently by the model with travel time residuals of 103 ms compared to 93 ms for all shots. The general trend with lower velocities in the west (Core Zone and southern Burwell domain) and higher velocities in the east (Nain Province and Komaktorvik shear zone) continues down to a depth of ~25 km, where the trend reverses and Core Zone velocities become higher than those in the Nain Province (Plate 1b).

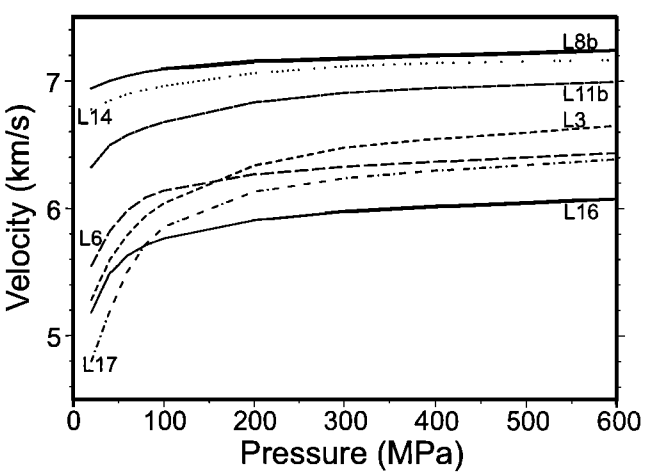

Figure 5. P wave velocity versus pressure for a selection of rock samples from the central Torngat Orogen. The sample locations are shown in Figure 2 and the lithologies are given in Table 1.

Plate 1 displays three cross sections overlain with results from the rock sample velocity measurements from the central Torngat Orogen. The E-W cross sections reveal that both the northern (Plate 1a) and the central Torngat Orogen (Plate 1b) have a preserved crustal root, although there is a significant change of the character of the root between the two parts of the orogen. In the north (Plate 1a) the root is shallower (~42 km) and narrower (~50 km) than in the south, where the maximum crustal thickness (Plate 1b) is 49 km. Velocities within the root are slightly lower in the north (7.1 km/s) than in the south (7.2 km/s), although this is at the limit of the resolution. Velocities within the root of the central Torngat Orogen have a Core Zone affinity ($v_p > 7.0$ km/s) rather than a Nain character, where lower crustal velocities are lower.

The N-S cross section (Plate 1c) through the study area summarizes the variations in crustal thickness. In the south, the Moho is as deep as 52 km but shallows to ~43 km before reaching the bend in the Abloviak shear zone and the Tasiuyak domain. In the southern Burwell domain the crustal thickness remains relatively constant around 42 km before decreasing to 35 km in the northern Burwell domain. In conjunction with the decrease of Moho depth in the northern Burwell domain, there is an increase in surface velocities forming the high-velocity region discussed earlier. The surface geology does not give an obvious reason for the high velocities, but the crustal thinning suggests Moho uplift in the northern Burwell domain associated with the exposure of deeper levels of crustal rocks at the surface.

All the velocity cross sections in Plate 1 show a change of the vertical velocity gradient within the crust. The upper crustal portion has a high gradient, while the lower crust is

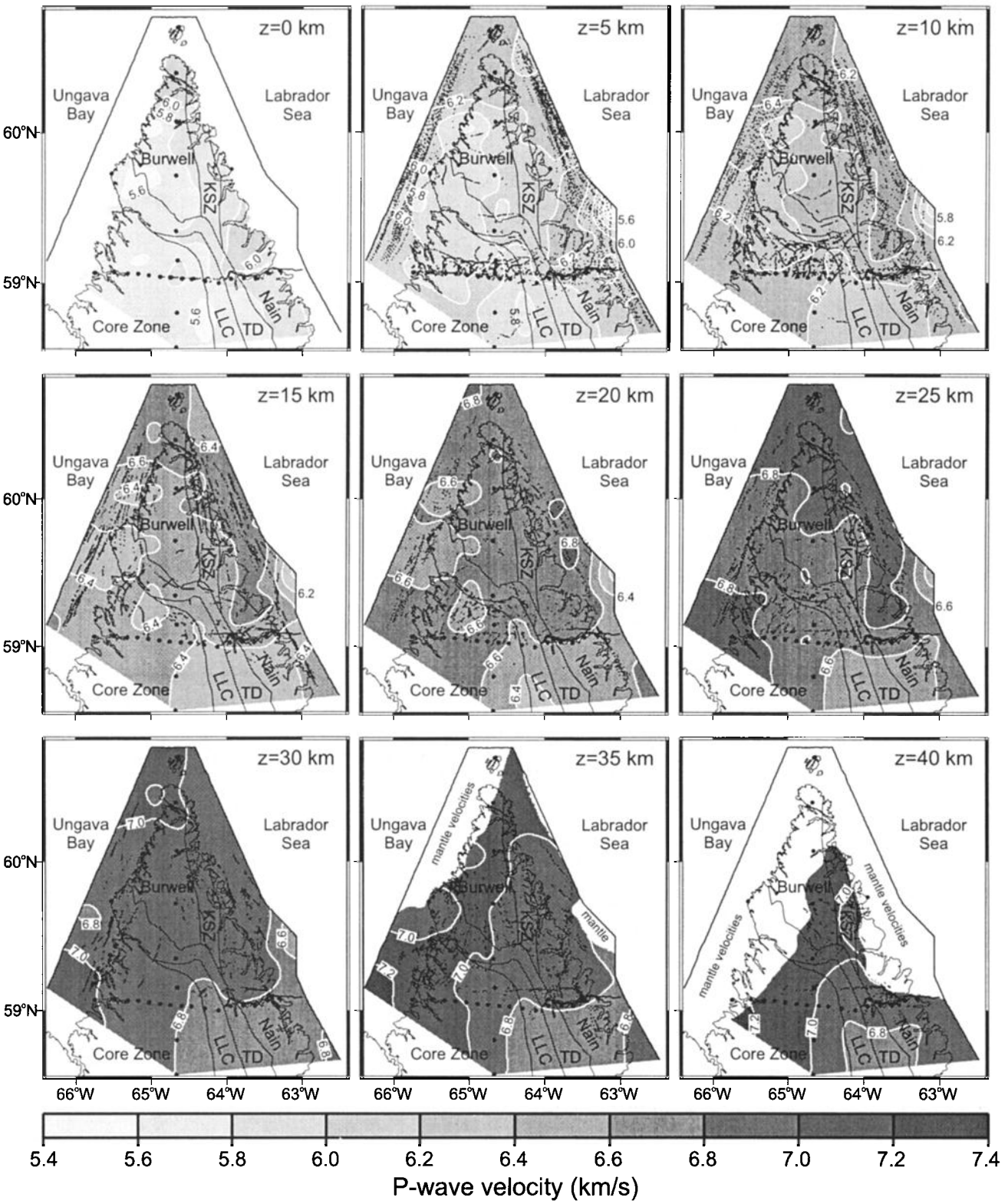

Figure 6. P wave velocity panels for horizontal cross-sections in the Torngat Orogen at depths ranging from 0 to 40 km. The contour interval is 0.2 km/s (white lines). Solid lines onshore mark the boundaries of the main geological provinces and the coastline. Solid lines offshore show the shot lines, and circles indicate the receiver locations. Solid dots show the location of rays crossing the depth level (indication for the ray coverage). KSZ is Komaktorvik shear zone, LLC is Lac Lomier complex, and TD is Tasiuyak domain.

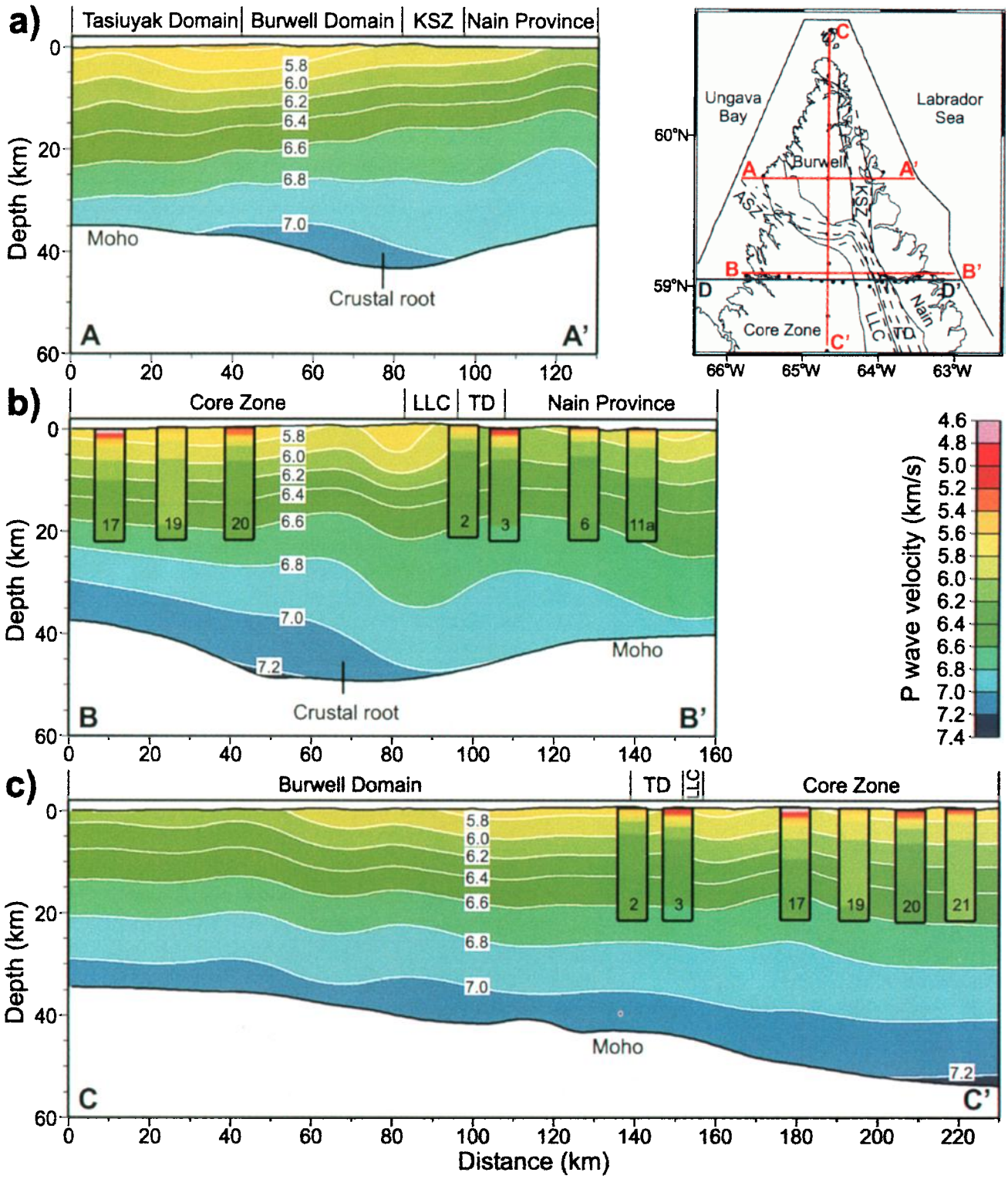

Plate 1. Velocity cross section (a) across the northern Torngat Orogen, (b) across the central Torngat Orogen, and (c) along a transect from the northern to the central Torngat Orogen. The contour interval is 0.2 km/s (white lines). Vertical velocity bars overlain on the cross sections represent the velocity-depth functions of rock samples from the central Torngat Orogen with the numbers identifying the sample. The inset shows the location of the cross sections (red lines), the receiver locations (circles), and the shot lines (black lines offshore). The blue line refers to the location of the cross section shown in Figures 7 and 8. KSZ is Komaktorvik shear zone, ASZ is Abloviak shear zone, LLC is Lac Lomier complex, and TD is Tasiuyak domain.

characterized by a low gradient. The transition from the high to the low gradient zone correlates approximately with the 6.6 km/s contour line. Results from 2-D forward models in the study area [*Funck and Louden*, 1998, 1999] show that the midcrustal boundary roughly coincides with the 6.6 km/s contour line and that there is a similar change of the velocity gradient at this level. Hence the change of the vertical velocity gradient in the tomographic results is interpreted as a first-order approximation for the midcrustal boundary (Conrad discontinuity) that divides the crust into upper and lower crust.

Comparison between rock sample velocities and results from the seismic tomography (Plate 1) shows a good agreement. Five samples were collected in the Core Zone, and the four gneissic samples (L17, L19-21, Table 1) match the velocities obtained from the tomography very closely with deviations in both directions. In contrast, the marble (L18) is characterized by velocities ~0.6 km/s higher than those of the gneisses and therefore is not a major component of the Core Zone crust. The paragneiss (L2) and felsic gneiss (L3) from the Tasiuyak domain have velocities compatible with the tomography. In contrast, two other gneisses from the Tasiuyak domain (L4 and L5) have velocities that are too low and too high, respectively. The latter rocks are common in the easternmost Tasiuyak domain, which is characterized by reworked gneisses. An appropriate mixture of these rocks may well fit the velocities determined by the tomography. However, the bulk of the Tasiuyak domain (according to the surface geology) is characterized by mainly mylonitic metasedimentary gneisses of which samples L2 and L3 are characteristic. Samples from the Nain Province show large ranges in velocity. The felsic gneisses (L10a, L10b, L11a, L13) and the anorthosite (L6) fit the velocity structure obtained from the tomography (Plate 1b). Dikes (L9, L14) and mafic gneisses (L8b, L11b, L15) have velocities that are too high to match the calculated upper crustal velocities. This indicates that felsic gneiss dominates relative to dikes and mafic gneiss for the entire upper crust, as it is for the surface.

The laboratory measurements can only be used to a certain degree to determine the bulk composition of the lower crust because it is uncertain whether or not the rock types sampled at the surface are representative for the lower crust. When extrapolating the velocities of the samples down to lower crustal levels, felsic rocks have rather too low a velocity to match the tomography results, whereas the velocities of the mafic samples are too high. This would suggest an intermediate composition of the lower crust as an initial approximation.

Rocks in the southern part of the Four Peaks domain (samples L7, L8b, and L9) show high velocities. The overall high velocities found within the Four Peaks domain are thought to be related to high density/velocity garnet-clinopyroxene-orthopyroxene granulites formed by high-pressure granulite facies metamorphism at paleodepths up to 1.3 GPa [*Van Kranendonk and Wardle*, 1997].

5.3. Moho Depth

As seen in the velocity cross sections (Plate 1), there are substantial variations in Moho depth beneath the Torngat Orogen. These changes are summarized in the depth-to-Moho map obtained from the tomographic inversion (Plate 2a). As noted above, the central Torngat Orogen is characterized by a 52-km-deep crustal root with a width of ~100 km similar to the previous 2-D model [*Funck and Louden*, 1999]. North of the bend in the Abloviak shear zone, the root narrows and shallows significantly with a maximum depth of 44 km and a width of ~45 km. Eventually, the root disappears north of 60°N. Crustal thickness outside the root area varies between ~33 and 40 km. In southern Ungava Bay the Moho depth is of the order of 38 km, compatible with other results [*Funck and Louden*, 1999]. In NE Ungava Bay, Moho depth is as low as ~33 km. Along the east coast of Labrador in the Nain Province, the crust is 40 km thick but thins seaward at the continental margin to 35 km at the limit of the mapped area.

The shape of the Moho surface correlates closely with the shear zones in the Torngat Orogen (Plate 2a). In the north the eastern limit of the root in the northern Torngat Orogen correlates with the eastern border of the Komaktorvik shear zone, while the western limit of the northern root correlates with another shear zone that converges from the southwest into the Komaktorvik shear zone. The root eventually disappears with the northward convergence of these two shear zones. To the south, the bend in the Abloviak shear zone separates the rather shallow root in the north from the deep root in the central Torngat Orogen. Farther south, the eastern border of the root follows the Abloviak shear zone.

5.4. Model Resolution and Uncertainty

Several tests have been carried out to determine quantitative estimates of the precision of the tomographic inversion. To check for the Moho depth, a test was performed with synthetic travel times computed from a model with the same Moho geometry and a similar velocity structure as in the final model. These travel times were inverted using the same inversion path and starting model as for the real data set. Comparison of the input Moho depth with the results obtained from the test show a deviation of the order of ±1 km with a maximum error of 2.5 km.

Another method was used to determine the Moho depth independently from the inversion program JIVE3D. For this purpose a Moho map was compiled based on normal move-out (NMO) corrections for the P_mP phase, assuming a constant velocity crust with a velocity of 6.55 km/s. This velocity was the average value found for the crust along the 2-D seismic transect across the central Torngat Orogen [*Funck and Louden*, 1999]. Comparison of travel times between a constant velocity crust and a layered 38-km-thick crust with the same average velocity shows that the travel times are fairly similar up to offsets of 180 km but then start to diverge. For this reason, only P_mP travel times for offsets <180 km were included in the NMO method. In addition, shots in regions of the Labrador Sea covered with up to 5 km of sediments also were excluded. The Moho depth was calculated using the formula $z=[(vt)^2-x^2]^{1/2}$, where z is the Moho depth, x is offset, t is travel time, and v=6.55 km/s. The reflection point at the Moho is the midpoint between shot and receiver. The data points were gridded and low-pass-filtered (removing wavelengths <15 km). The resulting map (Plate 2b) shows similar variation of Moho depths as the map obtained from tomography (Plate 2a). The northward narrowing and shallowing of the crustal root is reasonably well matched, although the root appears slightly narrower and shallower than indicated by the tomography. Such deviations occur preferentially in areas with a high Moho curvature [cf. *Funck*

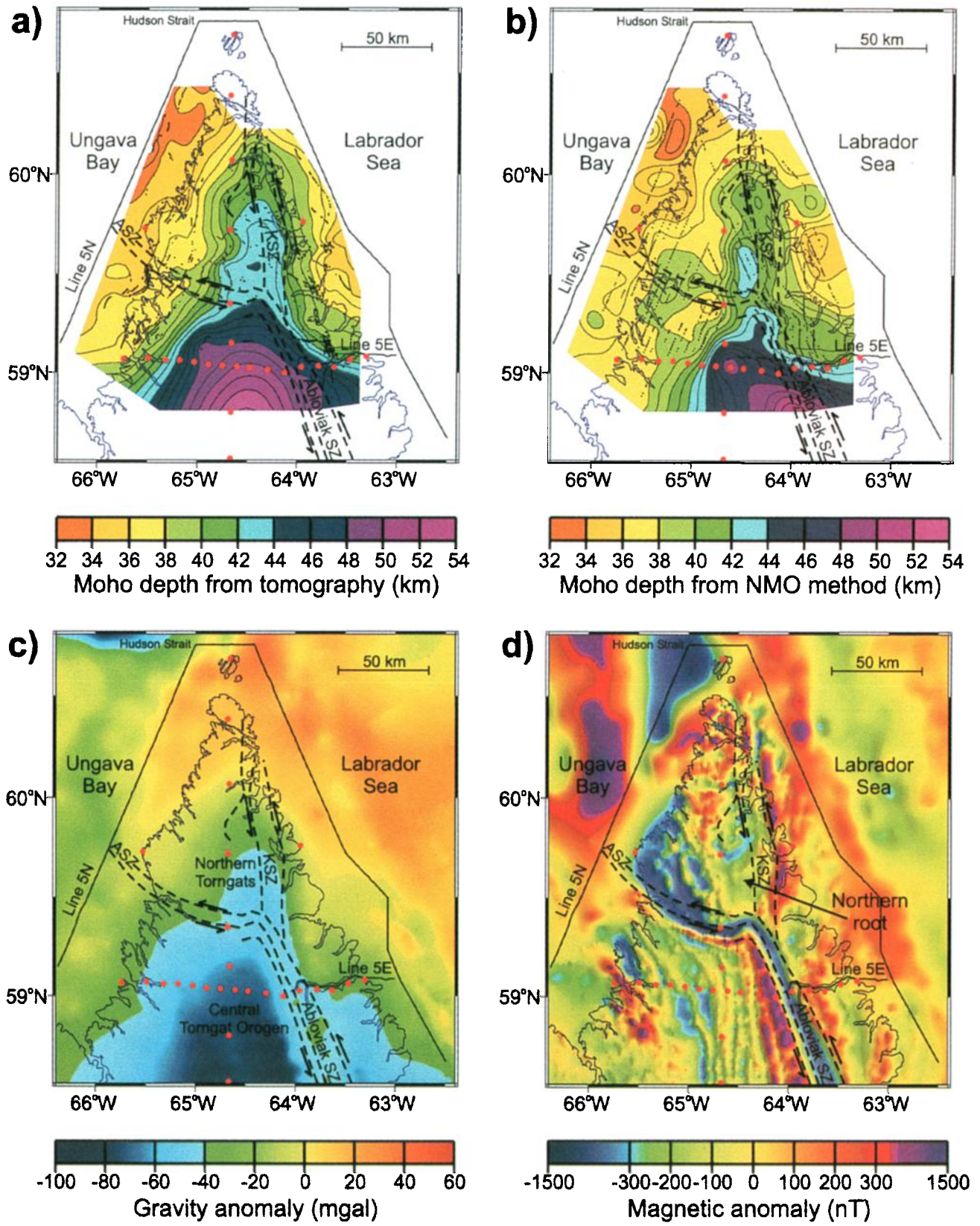

Plate 2. (a) Depth of the crust-mantle boundary (Moho) determined by seismic tomography. The contour interval is 1 km. (b) Depth of the crust-mantle boundary determined by NMO method (description in text). The contour interval is 1 km. (c) Gravity map. Values on land are Bouguer anomalies and in offshore areas are free-air anomalies. (d) Magnetic anomaly map. The shading is derived from illumination of the anomalies from the east. Dashed lines indicate the location of shear zones (ASZ, Abloviak shear zone; KSZ, Komaktorvik shear zone). Solid lines show the shot locations, and red circles represent the seismic receivers. Gravity in Ungava Bay was taken from Geosat and ERS-1 satellite altimetry (version 7.2 released by D. T. Sandwell and W. H. F. Smith), all other areas and magnetic data from Geophysical Data Centre of the Geological Survey of Canada.

et al., 1999] and can be well explained by the limitations inherent in the simplified NMO method.

To check for the lateral resolution of the model a checkerboard test [*Hearn and Ni*, 1994] was performed. The test shows that the distribution of shots and receivers is unable to resolve velocity perturbations south of 59°N because of the insufficient number of crossing ray paths. This is obvious in the horizontal cross sections (Figure 6) where the otherwise good correlation between contour lines and surface geology deteriorates south of 59°N. North of 59°N, lateral variations can be resolved down to a depth of ~25 km in areas with ray coverage (Figure 6). Below 25 km the tomography is only able to resolve lateral velocity perturbations in a 20-km-wide zone north of 59°N along the E-W line (Figure 7) with the close station spacing (stations 11 to 26). As typical for checkerboard tests, perturbations within high-velocity zones are better recovered than in the low-velocity zones.

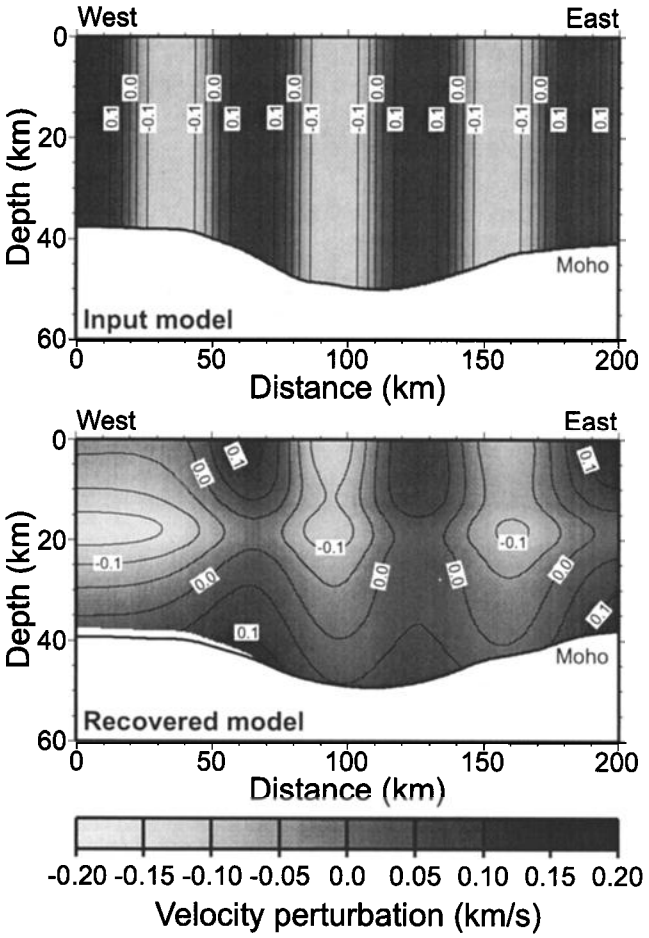

Figure 7. Checkerboard test along cross section shown in Figure 8. (top) Input model using the Moho geometry derived from the seismic tomography (Plate 2a) and a linear velocity function with 5.7 km/s at the surface, 6.6 km/s at a depth of 18 km, and 7.2 km/s at 50 km depth. In addition, the velocity was perturbed by ±0.15 km/s in vertical columns with a width of three velocity nodes (=20 km). Synthetic travel times for the same shot-receiver geometry as in the experiment were computed and inverted using the same inversion path as for the real data. (bottom) Recovered velocity perturbations. Contour interval is 0.05 km/s.

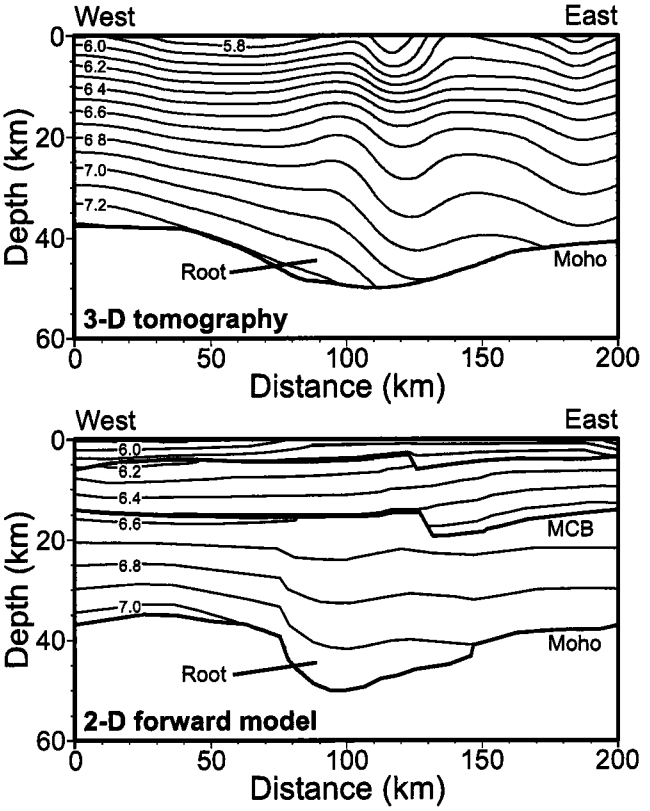

Figure 8. Comparison of velocity cross sections obtained (top) from 3-D tomography and (bottom) from 2-D forward model [*Funck and Louden*, 1999] of a R/WAR seismic line (bottom). The contour interval (thin solid lines) is 0.1 km/s, and layer boundaries are drawn by bold lines. The location of the cross section is shown as a blue line in the inset of Plate 1. MCB is midcrustal boundary.

A R/WAR seismic line [*Funck and Louden*, 1999] across the central Torngat Orogen (line 5W-E in Figure 1) allows for another comparison with the tomography (Figure 8). On the 2-D line with in-line shots it was possible to identify additional seismic phases allowing for a division of the crust into three layers. Velocity discontinuities occur at the layer boundaries, in particular at the midcrustal boundary (MCB). In contrast, the fan shots used in the tomography did not allow for such a subdivision of the crust because such additional phases could not be safely identified on most stations. The crustal velocity structure in the tomography is therefore continuous. However, the change of velocity gradient around the 6.6 km/s contour line fits well with the midcrustal boundary modeled along the 2-D seismic line. The deviations between the velocities in the two models generally do not exceed 0.2 km/s. The steps in the layer geometry mapped by the 2-D model at a distance of ~130 km seem to correspond to the eastern limit of the downward bend of velocity contour lines in the tomography. Differences in Moho depth between the two models are generally <3 km, with the largest deviation occurring at the western flank of the root. This zone is only sparsely covered by Moho reflections in the 2-D model, and out of plane reflections from the northward shallowing root may contribute to the discrepancies.

With the decrease of ray coverage with depth the possible trade-off between velocity and Moho depth needs to be

explored. The algorithm of JIVE3D and the inversion path were designed to extrapolate and interpolate velocity gradients from well-determined regions of the model to less constrained areas. This allows for an approximation of lowermost crustal velocities by knowing the velocities and gradients from upper portions of the lower crust, assuming that there are no compositional changes with depth. Comparison with the 2-D R/WAR seismic experiment (Figure 8) suggests that the velocity error is <0.2 km/s. A change of velocity in the lowermost crust by 0.2 km/s would affect the Moho depth by <1 km (i.e., at the resolution of the experiment) and would not change the overall pattern of the Moho geometry beneath the Torngat Orogen.

6. Discussion

6.1. Proterozoic Orogeny

Geological mapping and geochronological work conducted since 1991 by Lithoprobe's ECSOOT program (compare summary of *Wardle* [1998]) have greatly improved the understanding of the Torngat Orogen and provide the framework for the interpretation of the seismic data. The tomographic study presented in this paper provides information about the deeper crust in the transition zone between the northern and central Torngat Orogen that is a key region for the interpretation of the orogeny. It is here that the surface geology differs most prominently from a two-dimensional structure, where the bend of the Abloviak shear zone occurs and where the Burwell domain disappears to the south. The following discussion will first focus on the crustal root, following which a geodynamic model for the Torngat Orogen will be presented.

6.1.1. Crustal root. Previous knowledge about the crustal root was restricted to the R/WAR seismic line across the central Torngat Orogen that showed a 50-km-deep root [*Funck and Louden*, 1999], and a multichannel seismic line farther north in Hudson Strait [*Hall et al.*, 1995] that showed no evidence for a root. The results from the tomography provide a link between these two lines and put the root into context with the complex geology in the area. It was found that the deep root in the central Torngat Orogen correlates with the Abloviak shear zone, while the narrower and shallower northern root is bounded by the Komaktorvik shear zone and other shear zones that converge into the Komaktorvik shear zone. The linkage of the shear zones with the Moho geometry is evidence for the importance of the shear zones in the orogeny and also indicates that the shearing probably affected the entire crust, as already suggested for the Abloviak shear zone [*Funck and Louden*, 1999].

Mapping by *Van Kranendonk and Wardle* [1997] shows that the surface rocks above the northern root (eastern edge of Burwell domain) are at amphibolite facies, while the remainder of the Burwell domain to the west and north is characterized by granulite facies. This would suggest less uplift in the region of the root and therefore a deeper Moho, which is in agreement with the seismic results. This lateral facies distribution shows up very well in the magnetic map (Plate 2d). The area of the northern crustal root has fairly constant negative magnetic anomalies of around -200 nT, while the area outside the root is characterized by mainly positive anomalies. This change in magnetic properties is strongest across the eastern border of the Komaktorvik shear zone.

On the basis of gravity modeling along the R/WAR seismic line across the central Torngat Orogen, *Funck and Louden* [1999] noticed that the gravity low along the transect is related to the crustal root. They cautiously concluded that the gravity low beneath the central Torngat Orogen marks the outline of the crustal root. The new Moho map derived from the seismic tomography allows a more definitive correlation between the Moho depth (Plate 2a) and gravity anomalies (Plate 2c). Comparison between the gravity and the Moho geometry reveals an almost one-to-one correlation. The broad gravity low in the central Torngat Orogen narrows across the bend in the Abloviak shear zone, and its amplitude decays northward as the root disappears. Gravity highs in NE Ungava Bay and in the Labrador Sea correspond to shallower Moho depths.

Using this close correlation between the gravity anomaly and Moho depth, one can estimate the lateral dimensions of the root south of the study area (Figure 9). The gravity low in the central Torngat Orogen can be used as a proxy for the crustal root. To the northeast the low is bounded by the Abloviak shear zone, and to the southwest it is bounded by the Falcoz shear zone. Both shear zones were active during the D2 phase of deformation. To the south, the gravity low weakens and is overprinted by the signature of the 1.3 Ga anorogenic Nain Plutonic Suite (NPS) [*Emslie et al.*, 1994].

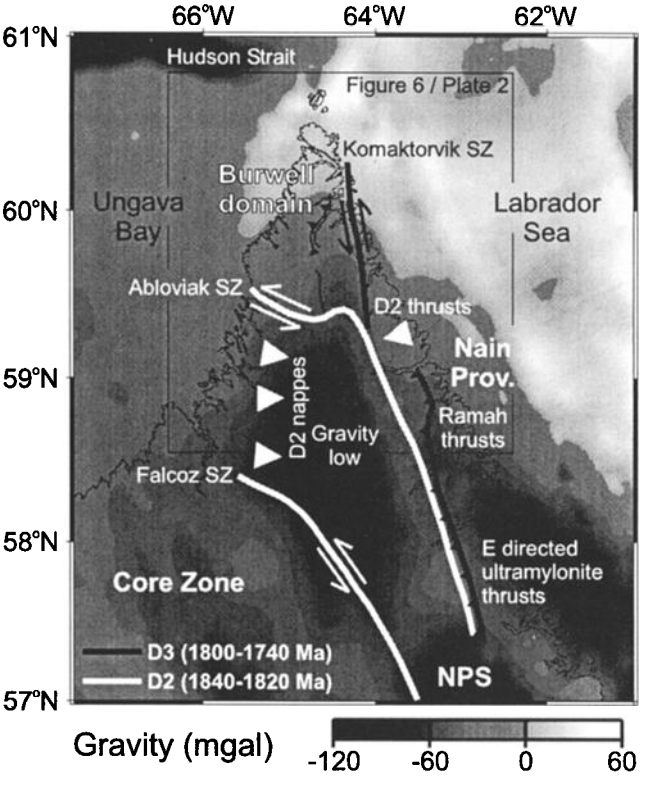

Figure 9. Gravity map of the Torngat Orogen shown together with geological features. Structures shown in black refer to deformation during the D3 phase (1800-1740 Ma) and those in white to the D2 phase (1840-1820 Ma). Arrows indicate the sense of displacement of the shear zones (SZ). NPS is Nain Plutonic Suite. Gravity in Ungava Bay was taken from Geosat and ERS-1 satellite altimetry (version 7.2 released by D. T. Sandwell and W. H. F. Smith). Data for the other areas were supplied by the Geophysical Data Centre of the Geological Survey of Canada.

Crustal thickness in the area of the NPS varies between 33 and 39 km [*Funck and Louden*, 2000] showing that the root in the central Torngat Orogen does not continue southward. However, since the anorthositic and granitic plutonism of the NPS postdates the orogeny by some 500 Myr, it appears at least possible that the root once did extend farther south and was reworked by the later plutonism. The maximum extent of the root in the central Torngat Orogen is ~120 km in the E-W direction and 200 km from north to south.

The preservation of the root in the central and northern Torngat Mountains is explained by the lack of postorogenic magmatic activity, suggesting that processes such as delamination did not occur and that the root was rapidly frozen in place. The lack of postorogenic magmatism is probably due to the depleted and refractory nature of the underlying Archean lithosphere which may have inhibited large-scale crustal melting during postcollisional delamination/slab breakoff and uplift [*Durrheim and Mooney*, 1994]. Since Early Proterozoic orogens such as the Torngat Orogen, the Trans-Hudson Orogen [*Lucas et al.*, 1993; *Németh et al.*, 1996] or Svecofennica [*Grad and Luosto*, 1987; *BABEL Working Group*, 1990] more commonly involve refractory Archean lithosphere, they are probably more likely to preserve their roots than younger orogens. *Zheng and Arkani-Hamed* [1998] modeled regional-scale gravity anomalies in NE Canada and found that the Moho beneath the Torngat Orogen has an excess undulation of 4-8 km compared with the undulation of an isostatically compensated Moho. In their model they suggest that the surface topography was compensated by a deep crustal root during or shortly after the collision. Later, the strong lower crust does not remain in isostatic balance during surface erosion, and the excess buoyancy of the root is supported by crustal strength.

6.1.2. Geodynamic model. The orogenic development of the Torngat Orogen is characterized by three deformational phases (D1-D3, Figure 10). Previously, the direction of subduction during the D1 phase was controversial. For the northern Torngat Orogen, eastward dipping subduction of the Core Zone beneath the Nain Province was inferred [*Wardle and Van Kranendonk*, 1996] on the basis of the intrusion of Burwell arc-type plutons into Nain Archean crust. In the central and southern Torngat Orogen the situation was more complicated since both the Core Zone and the Nain margins are intruded by magmatic suites. This was interpreted as resulting from double subduction or from a flip of subduction polarity from eastward to westward dipping subduction [*Wardle and Van Kranendonk*, 1996]. Preliminary geochronological work [*Scott*, 1995b] demonstrated that the western magmatic suite (Lac Lomier complex) was younger at circa 1.83 Ga than the Burwell arc and suggested that easterly subduction of circa 1.91-1.86 Ga age affected the entire western edge of the Nain Province. In contrast, *Funck and Louden* [1999] favored a model with westward dipping subduction or underthrusting to explain the geometry of the crustal root along the 2-D seismic transect across the central Torngat Orogen. However, the results from the tomography show that the velocities within the crustal root are more similar to the lower crustal velocities of the Core Zone, than those in the lower crust of the Nain Province (Plate 1b). Furthermore, the prominent asymmetry in the crustal root which led to the interpretation of westward underthrusting [*Funck and Louden*, 1999] is much less pronounced in the tomography (Figure 8). We suspect that the proximity of the 2-D transect to the bend in the Abloviak shear zone and the associated northward shallowing of the root may have resulted in off-plane reflections that produce artifacts on mapping of the Moho along the line. Alternatively, if the asymmetry of the root along the 2-D line is true, it may be related to later (D3) tectonism. In summary, results from the tomography favor eastward dipping subduction along the entire Nain margin (Figure 10a). This is also the present consensus based on geological data [*Wardle*, 1998; *Scott*, 1998]. Tectonic interpretations of the 2-D seismic data solely based on the layer geometry [*Funck and Louden*, 1999] seem to oversimplify the geological complexities in the region.

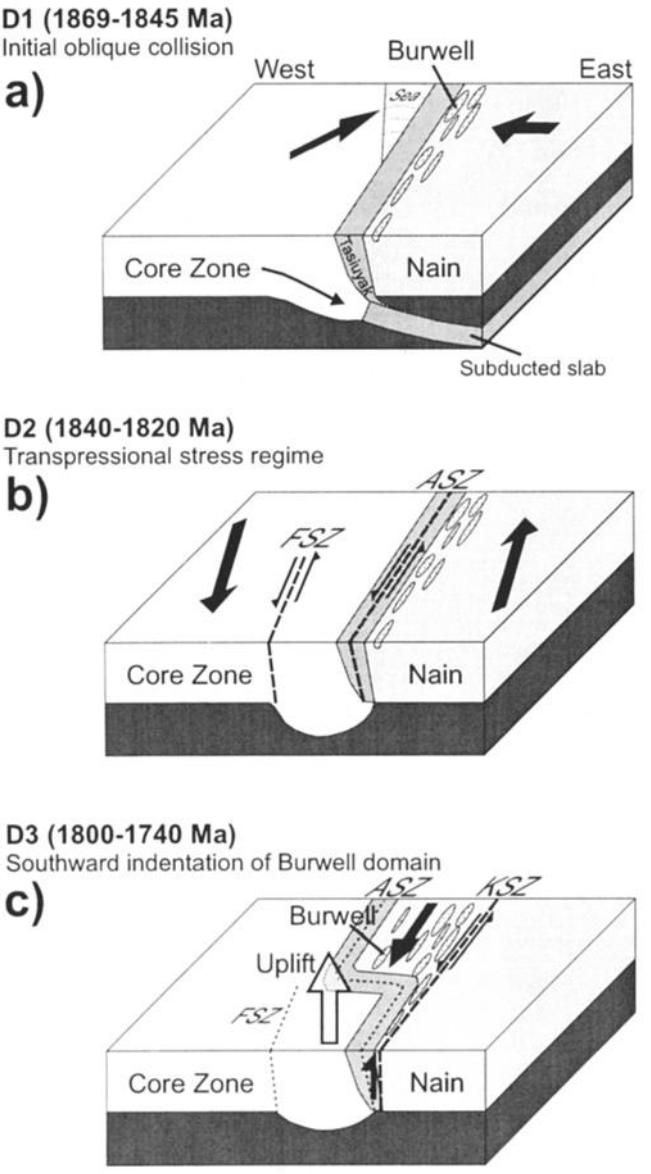

Figure 10. Geodynamic interpretation of the Torngat Orogen. (a) Eastward dipping subduction of Core Zone beneath Nain Province and initial oblique collision during D1 phase. (b) Transpressional stress regime during D2 phase with coeval Abloviak (ASZ) and Falcoz (FSZ) shear zones focusing strain in the area of the root. (c) Southward indentation of the Burwell domain during D3 phase resulting in bending of the Abloviak shear zone. This indentation was accommodated by the Komaktorvik shear zone (KSZ).

Close spatial correlation of the northern and central crustal root with D2 and D3 structures (Plate 2 and Figure 9) suggests that crustal thickening did not occur after D3. Beneath the central Torngat Orogen, all three phases of deformation might have contributed to the thickening, although there is evidence that the major phase of thickening occurred during D2 deformation (Figure 10b). A mechanism for D3 thickening could have been the west directed underthrusting of Nain crust beneath the Core Zone along thrusts east of the Abloviak shear zone. However, the Core Zone affinity of the root (Plate 1b) argues against a major contribution to the root by such a process. In addition, the orogen was uplifted at 1.8 Ga (beginning of D3) and greater uplift in the Core Zone of the central Torngat Orogen [*Scott*, 1998] could be explained by isostatic rebound of a preexisting (i.e., prior to D3) deep root in that area.

Possible formation of the root during initial collision (D1) has two weaknesses. (1) An early crustal root would be likely to suffer thermal relaxation during the accompanying magmatism, and (2) it is difficult to explain why the root is less developed in the north where there was less uplift than in the central Torngat Orogen. The remaining option is that the bulk of the southern root developed during D2 deformation. The results from the tomography and the correlation with the gravity low suggest that the root is largely sandwiched between the Abloviak and Falcoz shear zones (Figure 9). This is an area where D2 deformation was transpressional and sinistral shearing was associated with a strong component of westerly directed nappe-style folding [*Wardle and Van Kranendonk*, 1996; *Goulet and Ciesielski*, 1990] and possible thrusting that was focused between the two shear zones (Figure 10b). This scenario can be interpreted as a continued attempt from D1 collision to subduct the Core Zone crust beneath the Nain Province.

The northern Torngat Orogen lies outside the area of the focused D2 transpressional shearing. The northern root probably developed by oblique D2 burial of the Nain margin beneath a tilted section of the Burwell domain [*Van Kranendonk and Wardle*, 1997]. Since the outer perimeter of the root coincides with near vertical D3 faults and shear zones (Komaktorvik shear zone and splay, Plate 2a and Figure 9), a differential uplift origin is inferred for its present shape. As noted earlier, surface rocks above the root are at amphibolite facies, while the remainder of the Burwell domain is characterized by granulite facies [*Van Kranendonk and Wardle*, 1997], suggesting less uplift in that region of the root and a deepening Moho. Southward indentation of the Burwell domain (Figure 10c) to produce the bend in the Abloviak shear zone may have amplified the northern part of the root in the central Torngat Orogen. The southward indentation of the Burwell domain was accommodated by the Komaktorvik shear zone. Differential higher uplift in the central Torngat Orogen has likely removed most of the Burwell domain in the south [*Scott*, 1998], apart from some small areas (e.g., Ingrid group) interpreted to be possible equivalents to Burwell magmatism in the south [*Wasteneys et al.*, 1996].

6.2. Labrador Sea Rifting

The correlation of the tomography velocity model with Proterozoic surface geology is very strong. However, there are two exceptions from this correlation. The crustal thinning along the Labrador continental margin (Plate 2a) can be easily explained by the Mesozoic rifting in Labrador Sea. More puzzling is the reduced crustal thickness in NE Ungava Bay and northern Labrador. The crustal thinning and the associated high-velocity region (Plates 1c and 2a and Figure 5) in the northern Burwell domain do not correlate with Proterozoic geology, nor is there onshore evidence for later compressional tectonism. Despite this lack of onshore evidence, the opening of the Labrador Sea seems to be the only plausible explanation for the crustal thinning in the area. This is at least suggested by the smooth continuation of the gravity high along the Labrador coast across northern Labrador into NE Ungava Bay (Plate 2c). A look at the rifting history of the Labrador Sea is necessary to explain why this gravity high does not run parallel to the coast of Labrador but instead extends westward across land.

The opening of the Labrador Sea (Figure 11) took place in two phases [*Srivastava*, 1978; *Roest and Srivastava*, 1989; *Chalmers*, 1991; *Chalmers and Laursen*, 1995] with the first phase ending at magnetic anomaly 24R (~56 Ma). At that time the rift axis reached Baffin Island and extension was transferred from the Labrador Sea to Baffin Bay along the Ungava transform fault system [*Storey et al.*, 1998]. The second phase of spreading in Labrador Sea started at 55 Ma and died out between anomalies 20 and 13 (~48-36 Ma) [*Roest and Srivastava*, 1989]. Spreading in Baffin Bay occurred during this second phase with complex transform

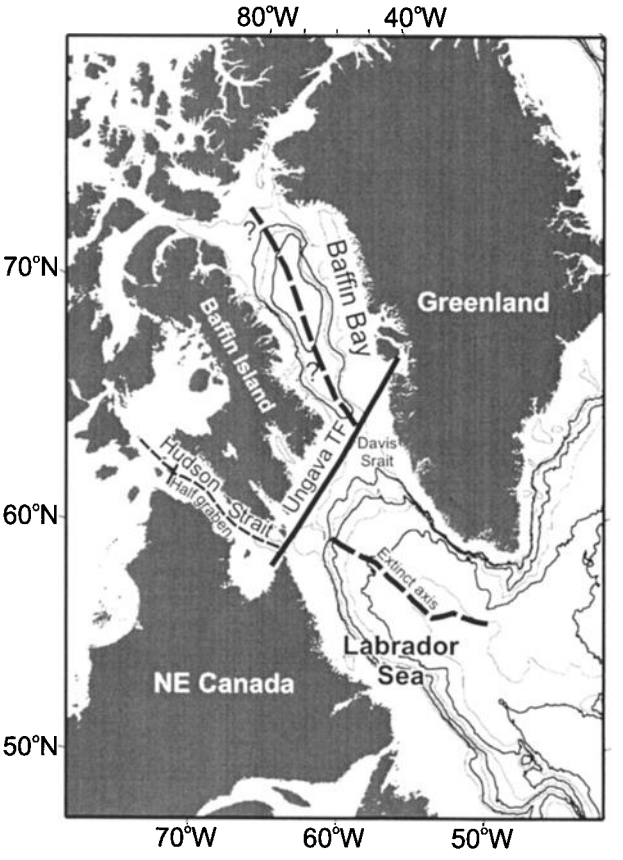

Figure 11. Rift system in the northwestern Atlantic Ocean. Bold dashed lines show the location of the extinct ridge axis in the Labrador Sea and the approximate axis in Baffin Bay. Thin dashed lines mark the half grabens in Hudson Strait, and the solid line shows the location of the Ungava transform fault (TF) system. The location of rifts is taken from *Roest and Srivastava* [1989] and *Kerr* [1981].

faults be developed in Davis Strait and Baffin Bay [*Roest and Srivastava*, 1989].

The plate reconstruction shows that the region with the reduced crustal thickness in northern Labrador and NE Ungava Bay was affected by the southwestern end of the Ungava fracture zone (Figure 11). Parts of the Ungava fault system (e.g., in West Greenland) were probably in net extension [*Storey et al.*, 1998; *Whittaker*, 1995]. In addition, half grabens along Hudson Strait [*Grant and Manchester*, 1970; *MacLean et al.*, 1986] are interpreted to be associated with rifting and spreading in the North Atlantic and Canadian Arctic [*Kerr*, 1981], although the exact age of the half graben structures is not known. In summary, spreading in the Labrador Sea developed some complexities when reaching Baffin Island. Transfer of the rifting along the Ungava fault system at 55 Ma into Baffin Bay and possible rifting in Hudson Strait resulted in crustal extension in northern Labrador and NE Ungava Bay.

It is interesting to note that the crustal thinning occurs just north of the crustal root in the northern Torngat Orogen. The root probably did not extend farther north because of its correlation with bounding Proterozoic shear zones and faults. Hence the crustal thickness and strength were probably reduced north of the root, thus defining a relatively weak zone, which was more likely to be affected by the later rifting than the strong region of the root. The root may therefore have influenced the rifting pattern in Labrador Sea, in particular the location of the Ungava fault.

7. Conclusions

The Moho map obtained from seismic tomography shows a 100-km-wide, 52-km-thick crustal root in the central Torngat Orogen. The root continues into the northern Torngat Orogen but experiences a significant narrowing and shallowing across a westward bend in the Abloviak shear zone, which divides the central from the northern Torngat Orogen. The maximum crustal depth in the north is 44 km, and the width of the root is ~45 km. The Proterozoic root eventually disappears in northernmost Labrador possibly because a relatively weak crust north of the root was affected by extension during the opening of the Labrador Sea. The minimum crustal thickness in the region affected by the extension is 33 km. The preservation of the root is explained by the absence of postorogenic magmatism in the northern and central Torngat Orogen, which prevented reworking or thermal relaxation of the root. This lack of late magmatism is probably related to the depleted and refractory nature of the Archean lithosphere underlying the Torngat Orogen. Since Early Proterozoic orogens more commonly involve such refractory lithosphere, they may be more likely to preserve their roots than younger orogens.

The crustal root shows a close correlation with a Bouguer gravity low, allowing for a southward extrapolation of the Moho depth based on gravity data until the gravity signature of the root becomes overprinted by the Nain Plutonic Suite. The Moho and gravity anomaly maps show that the location of the root in the central Torngat Orogen is bounded by the Abloviak and Falcoz shear zones. These are large shear zones that formed during the D2 transpressional phase of deformation. This suggests that crustal thickening in the central Torngat Orogen has been partitioned and focused by these two coeval shear zones, a process not yet reported from other Precambrian or Paleozoic orogens with preserved roots.

The root beneath the northern Torngat Orogen lies outside the zone of the focused transpression and is bounded by faults and shear zones formed during the last phase of deformation (D3). Differential uplift along these faults with less uplift in the root area has probably influenced the present shape of the northern root. This interpretation is consistent with the distribution of metamorphic grades of surface rocks and magnetic anomalies in the northern Torngat Orogen.

P wave velocities determined by seismic tomography follow closely the boundaries of geological units and are compatible with laboratory velocity measurement from rock samples collected in the study area. Upper crustal velocities in the Core Zone and Burwell domain are 0.1-0.2 km/s lower than those in the Nain Province. Core Zone velocities show a good agreement with gneissic rock samples and the upper crustal velocities in the Nain Province match velocities obtained from felsic gneisses and anorthosites. Velocities in the root of the central Torngat Orogen are of the order of 7.2 km/s and are similar to lower crustal velocities within the Core Zone, while lower crustal velocities in the Nain Province are <6.9 km/s. This observation is compatible with eastward dipping subduction of Core Zone crust beneath the Nain Province. This conclusion is opposite to the previous model obtained from the 2-D seismic line in the central Torngats [*Funck and Louden*, 1999] and underlines how the 3-D experiment has added significantly to the interpretation of the orogeny.

Acknowledgments. We thank Ian Reid and other members of the scientific party, officers and crew of CSS *Hudson* cruise 96-021 and the members of the land operations party, who helped to carry out the seismic experiment and the rock sampling. IRIS PASSCAL supported use of their REFTEK instruments. Geomatics Canada assisted in processing the GPS locations of the land stations. Bob Iuliucci helped in the operation of the high-pressure testing facility, and Bruce Mitchell helped with the processing of the seismic data at Dalhousie. We thank Satish Singh and Tim Minshull for their support with regard to the inversion code. John Hole, Stephen McNutt, and the Associate Editor are thanked for their detailed and helpful reviews. The Geophysical Data Centre, Geological Survey of Canada, supplied the gravity and magnetic data. This work was supported by the Lithoprobe program of the Natural Science and Engineering Research Council of Canada and Geological Survey of Canada. This is Lithoprobe contribution 1167.

References

BABEL Working Group, Evidence for Precambrian plate tectonics from seismic profiling in the Baltic Shield, *Nature, 348*, 34-38, 1990.

Bertrand, J.-M., J.C. Roddick, M.J. Van Kranendonk, and I. Ermanovics, U-Pb geochronology of deformation and metamorphism across a central transect of the Early Proterozoic Torngat Orogen, North River map area, Labrador, *Can. J. Earth Sci*, *30*, 1470-1489, 1993.

Birch, A.F., The velocity of compressional waves in rocks to 10 kilobars, 1, *J. Geophys Res., 65*, 1083-1102, 1960.

Birch, A.F., The velocity of compressional waves in rocks to 10 kilobars, 2, *J. Geophys. Res., 66*, 2199-2224, 1961.

Bridgwater, D., and L. Schiøtte, The Archean gneiss complex of northern Labrador: A review of current results, ideas and problems, *Bull. Geol. Soc. Den., 39*, 153-166, 1991.

Bridgwater, D., A. Escher, and J. Watterson, Tectonic displacement and thermal activity in two contrasting Proterozoic mobile belts from Greenland, *Phils. Trans. R. Soc. London, Ser. A, 273*, 513-533, 1973.

Chalmers, J.A., New evidence on the structure of the Labrador Sea/Greenland continental margin, *J. Geol. Soc. London, 148*, 899-908, 1991.

Chalmers, J.A., and K.H. Laursen, Labrador Sea: The extent of

continental and oceanic crust and the timing of the onset of seafloor spreading, *Mar Pet. Geol., 12*, 205-217, 1995

Dunphy, J.M., and T. Skulski, Early Proterozoic granitic magmatism in the Ungava and New Quebec orogens: The Narsajuaq Terrane and the De Pas Batholith, in *Eastern Canadian Shield Onshore-Offshore Transect (ECSOOT), Report of Transect Meeting*, edited by R J. Wardle and J. Hall, *Lithoprobe Rep. 45*, pp. 37-50, Univ. of B. C., Vancouver, Canada, 1995

Durrheim, R.J., and W.D Mooney, Evolution of the Precambrian lithosphere: Seismological and geochemical constraints, *J Geophys. Res., 99*, 15,359-15,374, 1994

Emslie, R.F , M A. Hamilton, and R.J. Thériault, Petrogenesis of a Mid-Proterozoic anorthosite-mangerite-charnockite-granite (AMCG) complex: Isotopic and chemical evidence from the Nain Plutonic Suite, *J. Geol., 102*, 539-558, 1994

Farra, V., Amplitude computation in heterogeneous media by ray perturbation theory: A finite element approach, *Geophys. J. Int., 95*, 135-147, 1990.

Funck, T., and K E. Louden, Wide-angle seismic imaging of pristine Archean crust in the Nain Province, Labrador, *Can J. Earth Sci., 35*, 672-685, 1998.

Funck, T., and K.E. Louden, Wide-angle seismic transect across the Torngat Orogen, northern Labrador: Evidence for a Proterozoic crustal root, *J. Geophys. Res., 104*, 7463-7480, 1999.

Funck, T , and K.E. Louden, Seismic imaging of the Torngat Orogen and the Nain Plutonic Suite, in *Eastern Canadian Shield Onshore-Offshore Transect (ECSOOT), Report of Transect Meeting*, edited by R.J Wardle and J Hall, *Lithoprobe Rep. 73*, pp. 20-37, Univ. of B. C., Vancouver, Canada, 2000.

Funck, T., K.E. Louden, and J.W Hobro, The crustal root beneath the Torngat Orogen: Results of a tomography study compared with a NMO method, *Lithoprobe Seismic Process Fac. Newsl 12*, pp. 24-29, Univ. of Calgary, Calgary, Canada, 1999.

Goulet, N., and A. Ciesielski, The Abloviak shear zone and the NW Torngat Orogen, eastern Ungava Bay, Québec, *Geosci. Can., 17*, 269-272, 1990.

Grad, M., and U. Luosto, Seismic models of the crust of the Baltic shield along the SVEKA profile in Finland, *Ann. Geophys., 5*, 639-650, 1987

Grant, A.C., and K.S. Manchester, Geophysical investigations in the Ungava Bay-Hudson Strait region of northern Canada, *Can. J. Earth Sci., 7*, 1062-1076, 1970.

Hall, J., R.J. Wardle, C.F. Gower, A. Kerr, K. Coflin, C.E. Keen, and P. Carroll, Proterozoic orogens of the northeastern Canadian Shield: New information from the Lithoprobe ECSOOT crustal reflection seismic survey, *Can. J Earth Sci., 32*, 1119-1131, 1995.

Hearn, T.M., and J.F. Ni, P_n velocities beneath continental collision zones: The Turkish-Iranian Plateau, *Geophys. J. Int., 117*, 273-283, 1994.

Hobro, J.W., Three-dimensional tomographic inversion of combined reflection and refraction seismic travel-time data, Ph.D dissertation, Univ. of Cambridge, Cambridge, England, 1999.

Isnard, H., M. Parent, M. Bardoux, J. David, C. Gariépy, and R.K Stevenson, U-Pb, Sm-Nd and Pb-Pb isotope geochemistry of the high-grade gneiss assemblages along the southern shore of Ungava Bay, in *Eastern Canadian Shield Onshore-Offshore Transect (ECSOOT), Report of Transect Meeting*, edited by R.J. Wardle and J Hall, *Lithoprobe Rep. 68*, pp. 67-77, Univ. of B C., Vancouver, Canada, 1998.

Kerr, J.W., Stretching of the North American Plate by a now dormant Atlantic spreading centre, in *Geology of the North Atlantic borderlands*, edited by J W. Kerr, A.J. Fergusson, and L.C Machan, *Mem. Can. Soc. Pet Geol., 7*, 245-278, 1981

Lucas, S B , A. Green, Z. Hajnal, D. White, J. Lewry, K. Ashton, W Weber, and R. Clowes, Deep seismic profile across a Proterozoic collision zone· Surprise at depth, *Nature, 363*, 339-342, 1993.

Machado, N., N. Goulet, and C. Gariépy, U-Pb geochronology of reactivated Archean basement and of Hudsonian metamorphism in the northern Labrador Trough, *Can. J. Earth Sci., 26*, 1-15, 1989.

MacLean, B., G.L. Williams, B.V. Sanford, R.A. Klassen, C. Blakeney, and A Jennings, A reconnaissance study of the bedrock and surficial geology of Hudson Strait, N W.T, in *Current Research, Part B, Pap. Geol. Surv Can., 86-1B*, 617-635, 1986

McCaughey, M., and S.C. Singh, Simultaneous velocity and interface tomography of normal-incidence and wide-aperture seismic traveltime data, *Geophys J Int , 131*, 87-99, 1997.

National Geophysical Data Center, Data announcement 88-MGG-02, Digital relief of the surface of the Earth, Natl. Oceanic and Atmos. Admin., Natl. Geophys. Data Cent., Boulder, Colo., 1988.

Németh, B., Z Hajnal, and S.B Lucas, Moho signature from wide-angle reflections: Preliminary results of the 1993 Trans-Hudson orogen refraction experiment, *Tectonophysics, 264*, 111-121, 1996.

Nironen, M., The Svecofennian Orogen: A tectonic model, *Precambrian Res., 86*, 21-44, 1997

Roest, W R., and S.P. Srivastava, Sea-floor spreading in the Labrador Sea: A new reconstruction, *Geology, 17*, 1000-1003, 1989

Ryan, B., T.E. Krogh, L. Heaman, U Scharer, S. Philippe, and G. Olivier, On recent geochronological studies in the Nain Province, Churchill Province and Nain Plutonic Suite, north-central Labrador, in *Current Research, Rep. 91-1*, pp. 257-261, Geol Surv., Newfoundland Dep. of Mines and Energy, St. John's, Canada, 1991.

Scott, D.J., U-Pb geochronology of a Paleoproterozoic continental magmatic arc on the western margin of the Archean Nain craton, northern Labrador, Canada, *Can. J. Earth Sci., 32*, 1870-1882, 1995a.

Scott, D J., U-Pb geochronology of the northeastern Rae Province, part 1, A preliminary report on the Lac Lomier complex, northern Labrador, in *Eastern Canadian Shield Onshore-Offshore Transect (ECSOOT), Report of Transect Meeting*, edited by R.J. Wardle and J Hall, *Lithoprobe Rep. 45*, pp. 122-128, Univ. of B. C., Vancouver, Canada, 1995b.

Scott, D.J., Geology, U-Pb, and Pb-Pb geochronology of the Lake Harbour area, southern Baffin Island: Implications for the Paleoproterozoic tectonic evolution of northeastern Laurentia, *Can. J. Earth Sci., 34*, 140-155, 1997.

Scott, D.J., An overview of the U-Pb geochronology of the Paleoproterozoic Torngat Orogen, northeastern Canada, *Precambrian Res , 91*, 91-107, 1998.

Scott, D.J., and G. Gauthier, Comparison of TIMS (U-Pb) and laser ablation microprobe ICP-MS (Pb) techniques for age determination of detrital zircons from Paleoproterozoic metasedimentary rocks from northeastern Laurentia, Canada, with tectonic implications, *Chem. Geol , 131*, 127-142, 1996.

Scott, D.J., and N. Machado, U-Pb geochronology of the northern Torngat Orogen, Labrador, Canada: A record of Palaeoproterozoic magmatism and deformation, *Precambrian Res., 70*, 169-190, 1995.

Scott, D J , and M.R St-Onge, Paleoproterozoic assembly of northeast Laurentia revisited: A model based on southward extrapolation of Ungava-Baffin crustal architecture, in *Eastern Canadian Shield Onshore-Offshore Transect (ECSOOT), Report of Transect Meeting*, edited by R.J. Wardle and J. Hall, *Lithoprobe Rep. 68*, pp. 134-147, Univ. of B. C., Vancouver, Canada, 1998.

Smith, W.H.F , and P. Wessel, Gridding with continuous curvature splines in tension, *Geophysics, 55*, 293-305, 1990.

Srivastava, S.P., Evolution of the Labrador Sea and its bearing on the early evolution of the North Atlantic, *Geophys. J. R. Astron. Soc., 52*, 313-357, 1978.

Storey, M., R.A. Duncan, A.K. Pedersen, L M. Larsen, and H.C. Larsen, $^{40}Ar/^{39}Ar$ geochronology of the West Greenland Tertiary volcanic province, *Earth Planet. Sci. Lett., 160*, 569-586, 1998.

Sutton, J S , B.E. Marten, A.M S. Clark, and I. Knight, Correlation of the Precambrian supracrustal rocks of coastal Labrador and southwest Greenland, *Nature, 238*, 122-123, 1972.

U.S Geological Survey, Global 30 arc second elevation data set, EROS Data Cent., Sioux Falls, S D., 1996.

Van Kranendonk, M.J., Tectonic evolution of the Paleoproterozoic Torngat Orogen: Evidence from pressure-temperature-time-deformation paths in the North River map area, Labrador, *Tectonics, 15*, 843-869, 1996.

Van Kranendonk, M.J., and R.J. Wardle, Crustal scale flexural slip folding during late tectonic amplification of an orogenic boundary perturbation in the Paleoproterozoic Torngat Orogen, northeastern Canada, *Can. J Earth Sci., 34*, 1545-1565, 1997.

Wardle, R.J., The southeastern Churchill Province: Towards synthesis, in *Eastern Canadian Shield Onshore-Offshore Transect (ECSOOT), Report of Transect Meeting*, edited by R.J Wardle and J. Hall, *Lithoprobe Rep 68*, pp. 224-244, Univ. of B. C , Vancouver, Canada, 1998

Wardle, R.J., and M.J. Van Kranendonk, The Palaeoproterozoic southeastern Churchill Province of Labrador-Quebec, Canada: Orogenic development as a consequence of oblique collision and indentation, in *Precambrian Crustal Evolution in the North Atlantic Region*, edited by T.S. Brewer, *Geol. Soc. Spec. Publ., 112*, 137-153, 1996.

Wasteneys, H.A., R.J. Wardle, T.E. Krogh, and I. Ermanovics, U-Pb geochronological constraints on the deposition of the Ingrid group and implications for the Saglek-Hopedale and Nain craton-Torngat Orogen boundaries, in *Eastern Canadian Shield Onshore-Offshore Transect (ECSOOT), Report of Transect Meeting*, edited by R.J. Wardle and J. Hall, *Lithoprobe Rep. 57*, pp. 212-228, Univ. of B. C., Vancouver, Canada, 1996.

Wessel, P., and W.H.F. Smith, Free software helps map and display data, *Eos Trans. AGU, 72*, 441, 445-446, 1991.

Whittaker, R.C., A preliminary assessment of the structure, basin development and petroleum potential offshore central West Greenland, *Grønl. Geol. Unders. Open File Rep., 95/9*, 31 p., 1995.

Zheng, Y., and J. Arkani-Hamed, Joint inversion of gravity and magnetic anomalies of eastern Canada, *Can. J. Earth Sci., 35*, 832-853, 1998.

T. Funck and K. E. Louden, Department of Oceanography, Dalhousie University, Halifax, Nova Scotia, Canada B4H 4J1. (tfunck@is.dal.ca; klouden@is.dal.ca)

J. Hall, Department of Earth Sciences, Centre for Earth Resources Research, Memorial University of Newfoundland, St. John's, Newfoundland, Canada A1B 3X5. (jhall@waves.esd.mun.ca)

J. W. Hobro, Bullard Laboratories, Department of Earth Sciences, University of Cambridge, Madingley Road, Cambridge CB3 0EZ, England, U.K. (hobro@esc.cam.ac.uk)

A. M. Muzzatti, Department of Earth Sciences, Dalhousie University, Halifax, Nova Scotia, Canada B3H 3J5.

M. H. Salisbury, Geological Survey of Canada, Bedford Institute of Oceanography, P.O. Box 1006, Dartmouth, Nova Scotia, Canada B2Y 4A2. (matts@agc.bio.ns.ca)

R. J. Wardle, Geological Survey, Newfoundland Department of Mines and Energy, P.O. Box 8700, St. John's, Newfoundland, Canada A1B 4J6. (rjw@zeppo.geosurv.gov.nf.ca)

(Received August 16, 1999; revised May 3, 2000; accepted June 14, 2000.)